Electronic Supplementary Material (ESI) for Dalton Transactions.

Supporting information

Exquisitely Constructing Hierarchical Carbon Nanoarchitecture Decorating with Sulfides for High−Performance Li−S Batteries

Experimental Section

Materials

Carbon nanotubes (CNTs) (C822928, 95%); cobalt hexahydrate nitrate $Co(NO_3)_2 \cdot 6H_2O$ (CAS No: 10026−22−9, 99.99%) and Na_2MoO_4 $2H_2O$ (CAS No: 10102−40−6, 99.99%) were purchased from the Chinese Academy of Science. 2−Methylimidazole (CAS No: 693−98−1, 98%); Polyvinylpyrroolidone (PVP) (CAS No: 9003−39−8, 99%); C_2H_5NB (CAS No: 62−55−5, 99%) and sublimed sulfur (S) (CAS No: 7704−34−9, 99.95%) were purchased from Aladdin Co. ltd. Ketjen black (KB) (ECP−600JD, 98%); Carbon black (super P) (MA−EN−CO−010212); Li_2S (MA−EN−EL−50016A, 99.99%); 1,3 dioxolane (DOL) (CAS No: 646−06−0, 99.95%); 1,2 dimethoxyethane (DME) (CAS No: 110−71−4, 99.95%); bistrifluoromethane sulfonimide lithium salt (LiTFSI) (CAS No: 90076−65−6, 99.9%); Lithium nitrate ($LiNO_{3)}$ (CAS No: 7790−69−4, 99.9%); N−methyl−2−pyrrolidone (NMP) (CAS No: 872−50−4, 99.9%) and polyvinylidene fluoride (PVDF) (MA−EN−BI−01, 99.95%) were purchased from Guangdong Canrd New Energy Technology Co. ltd. All chemicals were used as received without further purification.

Preparation modified separators

The modified separators were prepared by uniformly materials (90 wt%) and PVDF (10 wt%) in NMP. The obtained suspension was evenly dispersed by ultrasound, filtered by vacuum on a commercial polypropylene (PP) separator and vacuum drying at 60 ℃ for 12 h.

Visualized adsorption experiment of Lithium Polysulfides

The Li_2S_6 solution was prepared by mixing sulfur and Li_2S in a 5:1 molar ratio and adding them to a mixed solution of DOL/DME (1:1, *v*/*v*). The mixed solution was then kept under an Ar atmosphere with stirring at 60 ℃ to produce a Li_2S_6 solution (5 mM).

Subsequently, 10 mg each of CoS_2−NC−CNTs@MoS_2, CoS_2−NC−CNTs and MoS_2@CNTs powders were immersed in the as−prepared Li_2S_6 solution (1.0 mL), and the discoloration of the solution was recorded.

Cell measurements

Working electrodes were fabricated by coating different samples (CoS_2−NC−CNTs@MoS_2, CoS_2−NC−CNTs and MoS_2@CNTs) onto the carbon paper (CP) (the mass loading of active material is ca. 1 mg cm^{-2}), and Celgard 2500 PP separators were sandwiched between two working electrodes. The electrolyte consisted of a 0.1 M Li_2S_6 (20 μL) solution of DOL and DME (1:1 *v*/*v*). Cyclic voltammetry (CV) tests were performed on a VMP3 multichannel electrochemical workstation (Bio Logic, France) at various scan rates within a voltage window from −1.0 to 1.0 V.

A CR2025−type coin battery was assembled using C/S as the cathode, original PP or modified PP as the separator, Li sheet as the anode and a blank Li−S electrolyte containing 2 wt% $LiNO_3$ was added. The typical sulfur areal mass loading was approximately 1 mg cm^{-2} , and the electrolyte/sulfur ratio was 20 μL/mg. A cathode with a high sulfur loading was also prepared and tested. CV and electrochemical impedance spectroscopy (*EIS*) measurements were performed on a VMP3 multichannel electrochemical workstation (Bio Logic, France). Galvanostatic charge−discharge (GCD) tests were performed on the LAND battery test system over a range of 1.7−2.8 voltage.

Li_2S nucleation test

The Li_2S_8 solution was prepared by mixing sulfur and Li_2S in a 7:1 molar ratio and adding them to a mixed solution of DOL/DME (1:1, *v*/*v*). Experiments were performed

using CoS_2−NC−CNTs@MoS_2 (CoS_2−NC−CNTs or CP) as the working electrode, and Li sheet was used as the counter electrode with PP separators. 20 μL Li_2S_8 was added to the cathode side as the electrolyte, and 20 μL blank Li−S electrolyte containing 2 wt% $LiNO_3$ was applied on the other side. The cell was discharged to 2.06 V, and then the voltage was held at 2.05 V to nucleate Li_2S.

Preparation of the C/S positive electrode

To prepare the C/S positive electrode, KB and S in a mass ratio of 3:7 were thoroughly ground for 30 min and then heated at 155 ℃ for 12 h to melt the S. Subsequently, the cooled C/S composites, Super P and PVDF (8:1:1 mass ratio) were placed in a small amount of NMP, homogeneously dispersed using ultrasound, coated on aluminum foil and dried in a vacuum at 60 ℃ overnight before use. In addition, cathodes containing 3.8, 4.9 and 7.2 mg cm^{-2} of sulfur were prepared.

Measurement of the galvanostatic intermittent titration technique (GITT)

A protocol of a current pulse at 0.1 C for 40 min with 10 min of rest was used. The internal resistance could be quantified by the following relation equation:

$$IR\ (\Omega) = |\Delta V_{QOCV} - \Delta V_{CCV}| / I_{applied}$$

where $\Delta V_{QOCV-CCV}$ is the voltage difference between the points of quasiopen−circuit voltage (QOCV) and closed−circuit voltage (CCV), and $I_{applied}$ is the applied current.

Materials characterization

The X−ray diffraction (XRD) measurements were performed on a Rigaku D/max2600 X−ray diffractometer. The morphology and microstructure of the materials were observed by scanning electron microscopy (SEM, SU70, Hitachi, Japan) and

transmission electron microscopy (TEM, FEI, Tecnai TF20). X−ray photoelectron spectra (XPS, Thermo ESCALAB 250Xi) of the materials were obtained to analyze the elemental contents and valence.

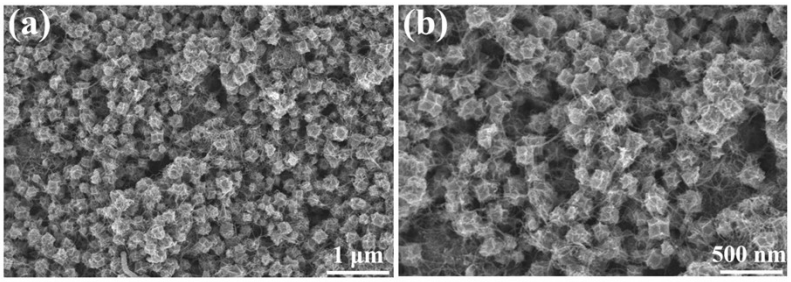

Fig. S1. (a, b) Low and high−magnification SEM images of CoS_2−NC−CNTs.

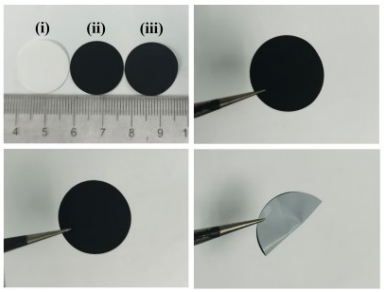

Fig. S2. Digital photography of the (i) PP, (ii) CoS_2−NC−CNTs−PP (iii) CoS_2−NC−CNTs@MoS_2−PP separators, and CoS_2−NC−CNTs@MoS_2−PP separator under bending and folding.

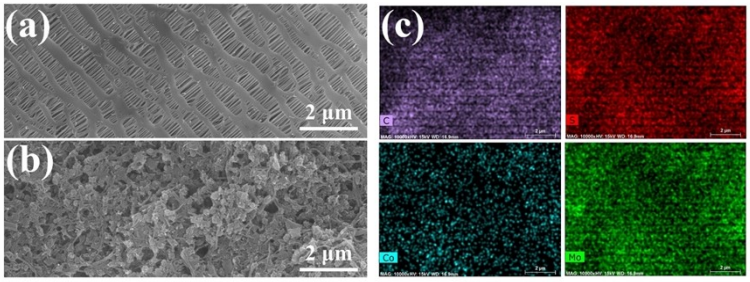

Fig. S3. (a, b) SEM images of the PP and CoS_2−NC−CNTs@MoS_2−PP separators. (c) EDS mapping imagery of the CoS_2−NC−CNTs@MoS_2−PP separator.

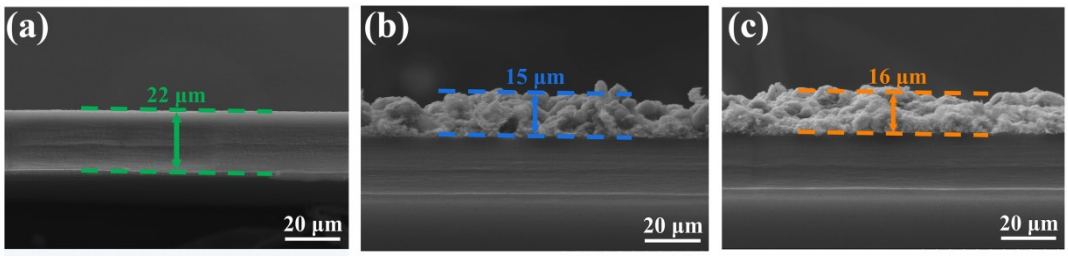

Fig. S4. (a–c) cross–sectional SEM images of the PP, CoS_2–NC–CNTs–PP and CoS_2–NC–CNTs@MoS_2–PP separators.

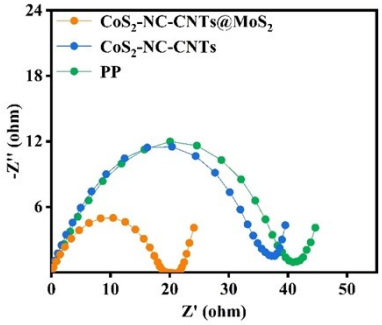

Fig. S5. *EIS* spectra of the developed materials in a symmetric cell.

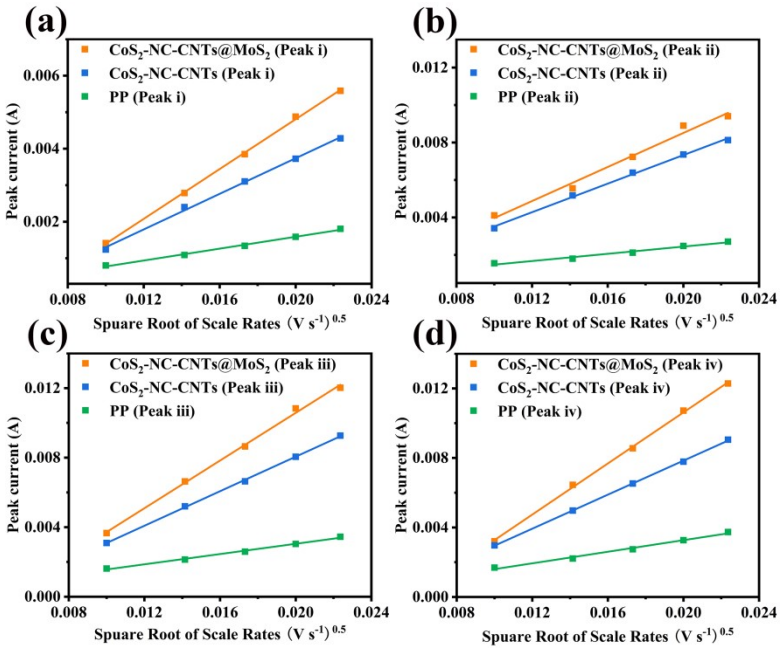

Fig. S6. (a−d) Linear relationship between peak current and the square root of the scan rates of four reduction peaks (Peak i, ii, iii and iv).

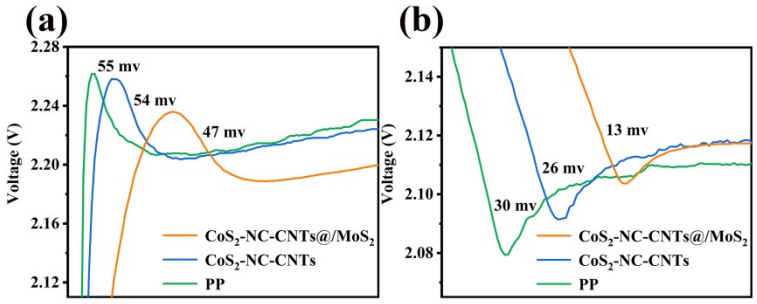

Fig. S7. Magnification of the initial charge−discharge curves of the batteries with different separators.

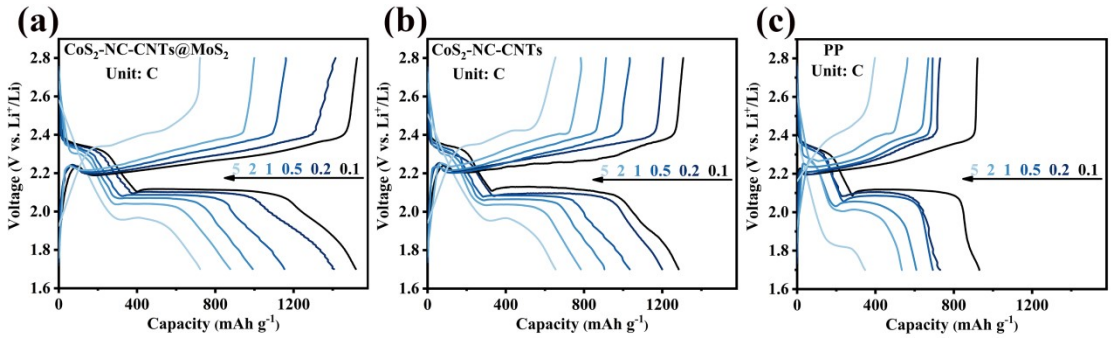

Fig. S8. Initial GCD curves of the CoS_2−NC−CNTs@MoS_2−PP, CoS_2−NC−CNTs−PP and PP cells at different current densities.

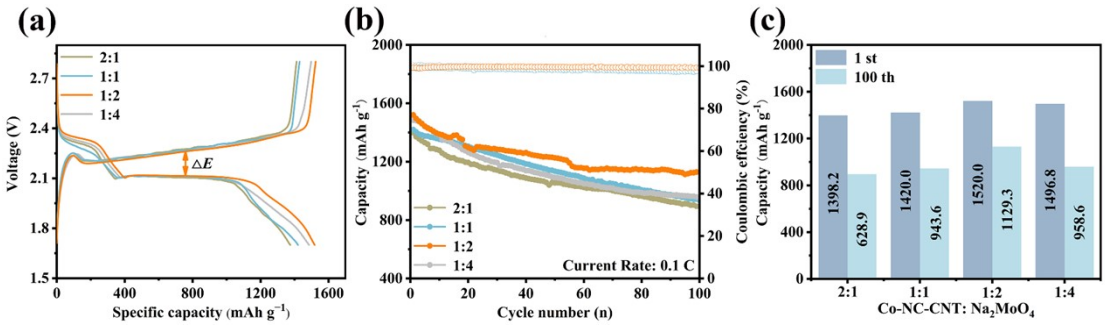

Fig. S9. (a) Initial GCD curves, (b) Cycling performance and (c) The first and 100th cycles of CoS_2−NC−CNTs@MoS_2−PP cells (with different ratio) at 0.1 C.

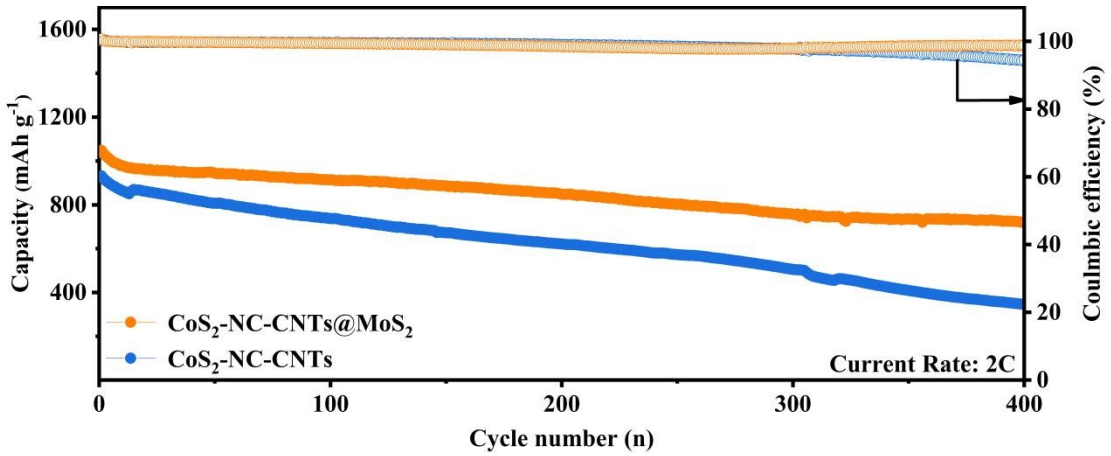

Fig. S10. Cycling performance of CoS_2−NC−CNTs@MoS_2−PP and CoS_2−NC−CNTs−PP cells at 2 C.

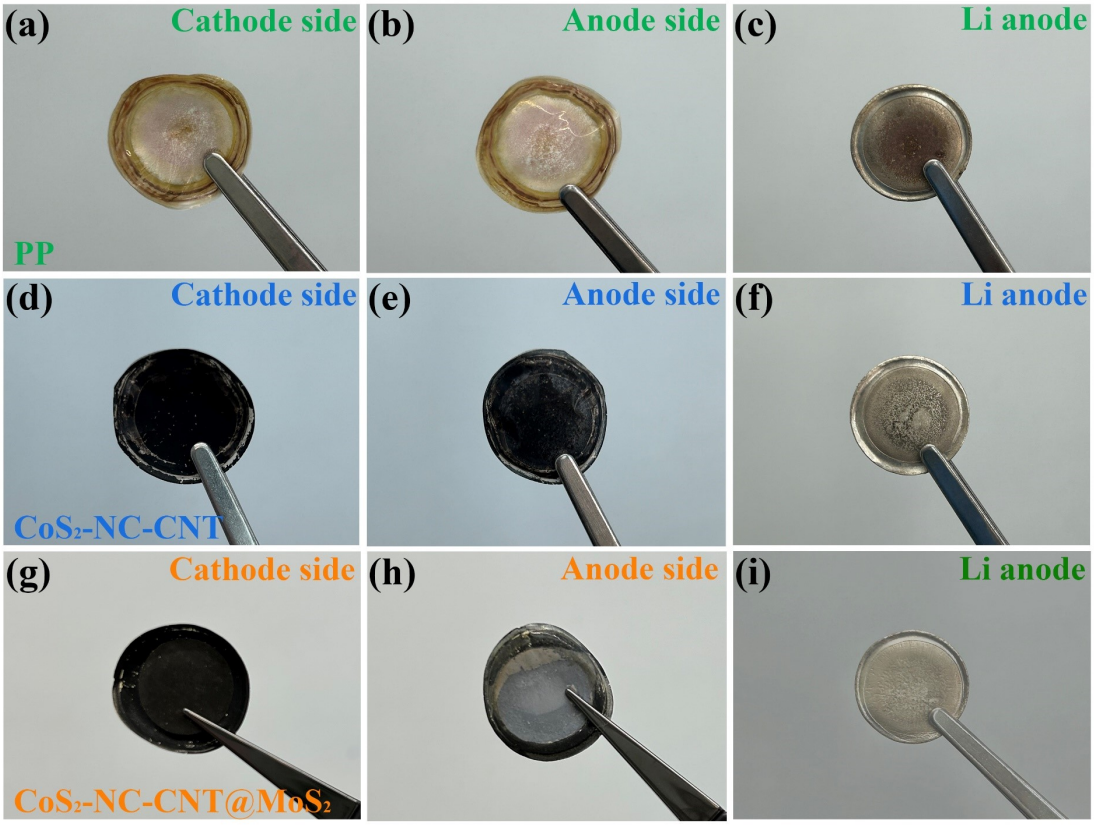

Fig. S11. Optical images of Li−S battery after cycling with different separators and Li anodes: (a−c) PP, (d−f) CoS_2−NC−CNTs−PP and (g−i) CoS_2−NC−CNTs@MoS_2−PP separators.

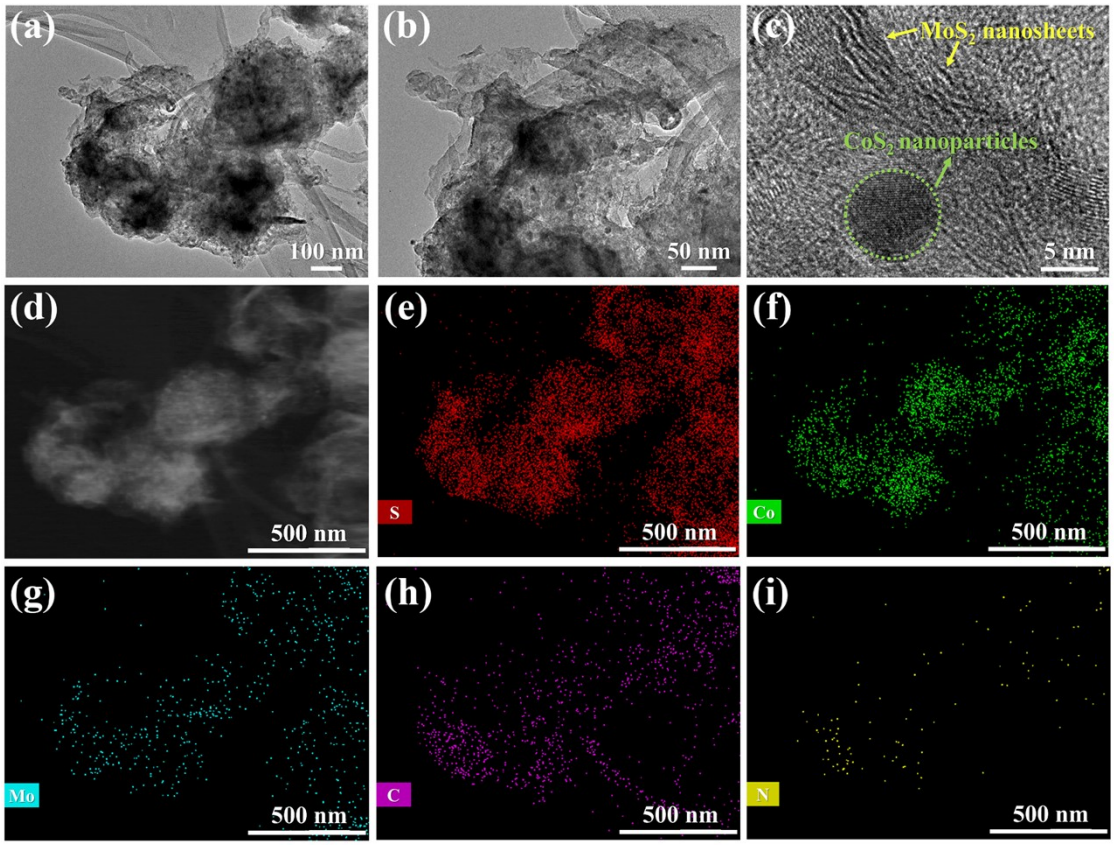

Fig. S12. (a–c) TEM and HR TEM images (d–i) HAADF−STEM and elemental mapping images of the CoS_2−NC−CNTs@MoS_2 after cycling.

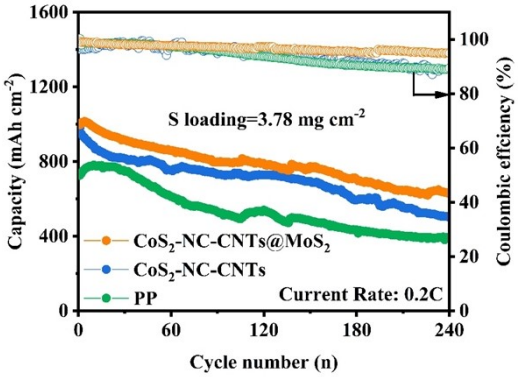

Fig. S13. Cyclic performance of the CoS_2−NC−CNTs@MoS_2−PP, CoS_2−NC−CNTs−PP and PP cells at 0.2 C with a mass loading of 3.78 mg cm^{-2} of sulfur cathodes.

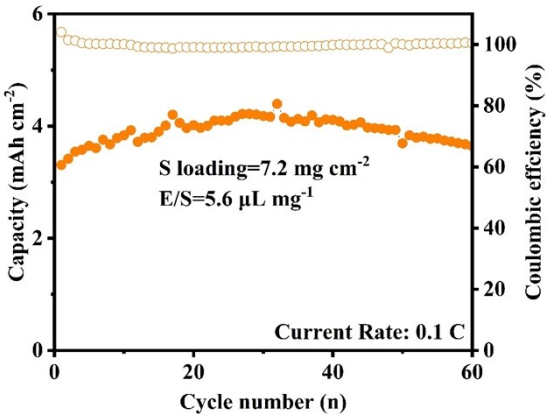

Fig. S14. Cycling performance of the CoS_2−NC−CNTs@MoS_2−PP separator battery under high sulfur load at 0.1 C.

Eqn. S1. The detailed calculation scheme for the lithium−ion diffusion rate.

The obtained CV curves can be used to calculate D_{Li+} from the Randles−Sevcik equation:

$$I_p = (2.65 \times 10^5) n^{1.5} A D_{Li+}^{0.5} C_{Li} v^{0.5} \quad (1)$$

where the peak current (I_p) of the CV curves are fitted for various scan rates and the square root of different scan rates ($v^{0.5}$). The slope of $I_{p\sim}v^{0.5}$ is positively correlated with D_{Li+}.

Eqn. S2. Detailed calculation scheme of the relative activation energy.

CV tests were performed at a scan rate (0.1 mV s^{-1}) as shown in Fig. 5a. Correspondingly, the relationship between the electrode potential and the activation energy over the different batteries can be calculated according to the equation:

$$E_a = E_a^0 + \alpha z F \varphi_{cathode}(Ox|Red)_{IR} \quad (2)$$

where E_a is the activation energy of the reduction process, E_a^0 is the intrinsic activation energy, α is the symmetry coefficient, z is the number of charge transferred, F is the Faraday's constant, and $\varphi_{cathode}(Ox|Red)_{IR}$ is the irreversible potential during cycling.

Tafel curve calculation formula:

$$\eta_{cathode} = \frac{RT}{\alpha z F} ln j_0 - \frac{RT}{\alpha z F} ln j_{cathode} \quad (3)$$

where $\eta_{cathode}$ is the overpotential of the cathode, j_0 is the exchange current density, and $j_{cathode}$ is the current at the cathode. The equation can be written in a more concise form:

$$\eta_{cathode} = a + b\ ln j_{cathode} \quad (4)$$

$$b = -\frac{RT}{\alpha z F} \quad (5)$$

where a is the intercept of the Tafel curve, and b is the slop of the Tafel curve.

Therefore, the equation (2) can be written as:

$$E_a = E_a^0 - \frac{RT}{b} \varphi_{cathode}(Ox|Red)_{IR} \quad (6)$$

Based on the intercept and slop of the Tafel curve in Figs. 5b–d, the activation energy during the discharge and charge process can be calculated.

The activation energy corresponding to the reduction of S_8 to the Li_2S_n:

PP separator battery: $E_{a1} = E_a^0 - 162.1$ kJ mol^{-1}

CoS_2–NC–CNTs@MoS_2 separator battery: $E_{a1}' = E_a^0 - 189.5$ kJ mol^{-1}

CoS_2–NC–CNTs separator battery: $E_{a1}'' = E_a^0 - 177.1$ kJ mol^{-1}

The difference in the activation energy can be calculated by subtracting the activation energy.

$\Delta E_i = E_{a1} - E_{a1}' = (E_a^0 - 162.1) - (E_a^0 - 189.5) = 27.4$ kJ mol^{-1}

$\Delta E_i' = E_{a1} - E_{a1}'' = (E_a^0 - 162.1) - (E_a^0 - 177.1) = 14.9$ kJ mol^{-1}

The activation energy of Li_2S_n to Li_2S:

PP separator battery: $E_{a2} = E_a^0 - 154.9$ kJ mol^{-1}

CoS_2−NC−CNTs@MoS_2 separator battery: $E_{a2}' = E_a^0 - 193.0$ kJ mol^{-1}

CoS_2−NC−CNTs separator battery: $E_{a2}'' = E_a^0 - 181.1$ kJ mol^{-1}

$\Delta E_{ii} = E_{a2} - E_{a2}' = (E_a^0 - 154.9) - (E_a^0 - 193.0) = 38.1$ kJ mol^{-1}

$\Delta E_{ii}' = E_{a2} - E_{a2}'' = (E_a^0 - 154.9) - (E_a^0 - 181.1) = 26.2$ kJ mol^{-1}

The activation energy of Li_2S to Li_2S_n:

PP separator battery: $E_{a3} = E_a^0 - 157.4$ kJ mol^{-1}

CoS_2−NC−CNTs@MoS_2 separator battery: $E_{a3}' = E_a^0 - 307.6$ kJ mol^{-1}

CoS_2−NC−CNTs separator battery: $E_{a3}'' = E_a^0 - 233.3$ kJ mol^{-1}

$\Delta E_{iii} = E_{a3} - E_{a3}' = (E_a^0 - 157.4) - (E_a^0 - 307.6) = 150.2$ kJ mol^{-1}

$\Delta E_{iii}' = E_{a3} - E_{a3}'' = (E_a^0 - 157.4) - (E_a^0 - 233.3) = 75.9$ kJ mol^{-1}

Table S1. Atomic ratio of the product obtained by ICP−OES

Element	Element content/ppm	Atomic ratio
Co	3.857	1
Mo	18.67	4.8

Table S2. Diffusion coefficients of Li^+ (D_{Li+}) of CoS_2−NC−CNTs@MoS_2−PP, CoS_2−NC−CNTs−PP and PP cells are calculated based on the Randles−Sevcik equation.

Samples	D_{Li+} (cm^{-2} s^{-1})			
	i	ii	iii	iv
CoS_2−NC−CNTs@MoS_2	2.25×10^{-8}	2.99×10^{-8}	4.51×10^{-8}	4.84×10^{-8}
CoS_2−NC−CNTs	1.61×10^{-8}	2.51×10^{-8}	3.27×10^{-8}	3.22×10^{-8}
PP	0.54×10^{-8}	0.63×10^{-8}	0.97×10^{-8}	1.09×10^{-8}

Table S3. Performance comparisons of the CoS_2−NC−CNTs@MoS_2 with representative high−performance catalysts for Li−S batteries[1−7].

Ref.	Sample	Sulfur loading (mg cm^{-2})	Rate	Cycles	Initial capacity (mAh g^{-1})	Capacity decay rate (%)
	This work	1	1	500	1079	0.076
			5	−	724.9	−
1	C−$MoSe_{2-x}$	1.1	1	500	854.9	0.09
2	DC/A O−CoVSe	1	5	−	683.8	−
3	CoRu@N−CNTs	1.34	1	400	1134.2	0.09
			3	−	686	−
4	Ni−Cu@C/HC	1	1	500	1202.2	0.088
			2	−	771.6	−
5	Co_3Fe_7/$Co_{5.47}N$	1.1	1	500	1054	0.075
			3	−	789	−
6	MoC NCs	1.3	1	600	946.7	0.076
			5	−	701	−
7	Bi_2Se_3	1	1	500	919.8	0.086

References

[1] Z. Nie, F. Xu, H. Liu, H. Wang, Y. Jiao, W. Zhu, Q. Wang, Y. Yan and J. Zhu, Chem. Eng. J., 2023, 481, 148433.

[2] P. Tan, Y. Yin, D. Cai, B. Fei, C. Zhang, Q. Chen and H. Zhan, J. Mater. Chem. A, 2024, DOI: 10.1039/D3TA07189H.

[3] P. Xia, S. Li, L. Yuan, S. Jing, X. Peng, S. Lu, Y. Zhan and H. Fan, J. Membr. Sci., 2024, 694, 122395.

[4] B. Zhang, J. Qie, W. Wang, Y. Li, Y. Cao, Y. Mao, J. You, C. Li and Z. Xu, Chem. Eng. J., 2024, 480, 148022.

[5] P. Wan, X. Peng, S. Dong, X. Liu, S. Lu, Y. Zhang and H. Fan, J. Colloid Interface Sci, 2024, 657, 757-766

[6] X. Zhang, M. Lei, S. Tian, J. Wang, Rare Met., 2023, 1-11.

[7] M. Zhao, J. Fu, D. Cai, C. Zhang, B. Fei, Y. Zhang, B. Sa, Q. Chena and H. Zhan, J. Mater. Chem. A, 2023, 11, 24089